Applications in Engineering Science 9 (2022) 100081

Contents lists available at ScienceDirect

Applications in Engineering Science

journal homepage: www.elsevier.com/locate/apples

Transition between partially and fully delaminated configurations of glued thin films

G. Napoli [a,*], G. Puglisi [b]

[a] Dipartimento di Matematica e Fisica "Ennio De Giorgi", Università del Salento, Lecce, Italy
[b] Dipartimento di Ingegneria Civile, Ambientale, del Territorio, Edile e di Chimica (DICATECh) Politecnico di Bari, Bari, Italy

ARTICLE INFO

Keywords:
Delamination
Instabilities
Capillary adhesion
Buckling
Euler's elastica

ABSTRACT

The insurgence of delamination phenomena of glued slender devices represents a diffuse drawback in numerous technological applications and it is diffusely observed in several biomechanical systems. Starting from the classical Euler elastica, we study the delamination of an inextensible elastic rod, with an end–end confinement, adhered to a rigid flat substrate. This system represents also a prototypical scheme mimicking decohesion induced by differential growth. Using energetic considerations, we draw a phase diagram between two classes of solutions: partially adhered and fully detached equilibrium states. We highlight a discontinuous transition between these two configurations, triggered by the confinement ε and regulated by the ratio between the elastocapillary length ℓ_{ec} and the length of the rod L. Eventually, we provide the approximate formula $\varepsilon_{cr} \approx L^2/(27\pi^2\ell_{ec}^2)$, in very good agreement with the numerical results.

1. Introduction

The delamination of thin sheets from an adhesive substrate represents a widespread problem observed in numerous branches of materials and structure engineering (Ke et al., 2010; Domokos et al., 2003; Petrik et al., 2020) and it is also the basis of several effects in biological sciences (Wyatt et al., 2020; Douglas et al., 2014; Goriely, 2017; Pocivavsek et al., 2018). Such instability represents generally an inconvenience to be avoided in various technological applications, since it potentially leads to device deterioration or breakage. However, its control and reversibility proposes a new paradigm, paving the way for a new generation of electronic devices and mechanical actuators (Sun et al., 2006; Kim et al., 2020; Lu and Kim, 2020). Thus, the possibility of reversible and controlled decohesion (Maddalena et al., 2009; Wu et al., 2011a,b) can be, as schematized in this paper, a key step toward the design of new adhesion-based actively controlled systems (Wang and Yamamoto, 2017). Similar phenomena have been speculated in Puglisi and Truskinovsky (2013) as mechanisms able to explain the strong reversible adhesion observed in biological systems.

The deformation of the delaminated components is often large so that linear theories are inappropriate to describe such effects. Previous analyses, which employ the Euler's *elastica*, studied delamination effects from various types of adhesive substrates such as flat, wet rigid surfaces (Majidi, 2007; Wagner and Vella, 2013), or soft solids (Vella et al., 2009; Oshri et al., 2018; Oshri, 2020). The same scheme can also be applied to study delamination in hard and soft confined strips (Cerda and Mahadevan, 2005; De Pascalis et al., 2014; Napoli and Goriely, 2017; De Tommasi et al., 2021; Maddalena et al., 2012; Coclite et al., 2019; Turzi et al., 2021). The Euler's elastica offers the invaluable feature of integrability of equilibrium equations, letting semi-analytical results with solutions in closed form and leading to a clear description of physical phenomena that cannot be achieved within classical linearized approaches.

More specifically, with respect to the phenomenon of decohesion buckling of interest in this paper, we recall that in Wagner and Vella (2013) it has been shown that Euler's elastica well describes quantitatively the delaminated shape for deflections with large slope and, hence, geometrically nonlinear. However, under the considered inextensibility assumption, the compressive stress required to induce delamination is theoretically unbounded. Thus, to describe the transition between the fully attached state and the delaminated configurations with finite-size blisters, due to either a finite compressive load (Napoli and Turzi, 2015) or body accretion (Napoli and Turzi, 2017), the theory of nearly inextensible rods has been successfully considered. Furthermore, the analysis in Wagner and Vella (2013) has recently been extended, including again weak rod compressibility, to take into account also of folded configurations with self-contact points (Davidovitch and Démery, 2021).

Our analysis goes in the direction of completing the one in Wagner and Vella (2013), considering the possibility of having a completely

* Corresponding author.
E-mail addresses: gaetano.napoli@unisalento.it (G. Napoli), giuseppe.puglisi@poliba.it (G. Puglisi).

https://doi.org/10.1016/j.apples.2021.100081
Received 30 November 2021; Received in revised form 17 December 2021; Accepted 22 December 2021
Available online 29 December 2021
2666-4968/© 2022 Published by Elsevier Ltd This is an open access article under the CC BY-NC-ND license (http://creativecommons.org/licenses/by-nc-nd/4.0/).

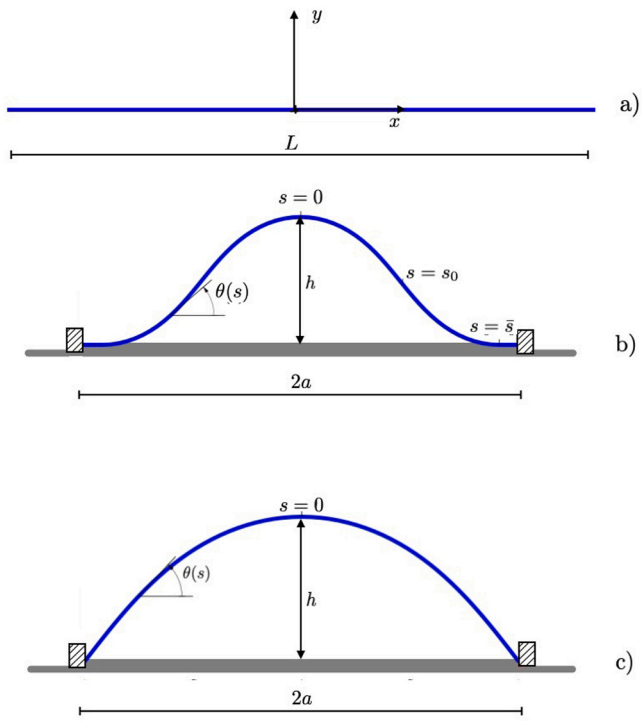

Fig. 1. Scheme of the possible delamination configurations of an elastic rod. (a) Undeformed beam, (b) blister configuration, (c) fully detached state.

delaminated solution with only the ends in contact with the substrate and describing the important effect of a *discontinuous* transition between partially attached configurations, characterized by finite blisters, to fully delaminated states. Our energetic approach let us attain a clear physical description of the phenomenon that is summarized in a phase diagram. In particular the transition is triggered by the confinement ε and the critical threshold is regulated by one single parameter $\xi_{\rm ec}$, measuring the relevance of elastic versus adhesion energy. We speculate that the obtained controllable bifurcation system can be adopted in actuation or sensing devices, by tuning either $\xi_{\rm ec}$ –e.g. through classical electroadhesion procedures (Shintake et al., 2016)– and ε –through a thermal (Que et al., 1999) or growth control as in the recently proposed approach in Arazoe et al. (2016)–.

2. Equilibrium configurations

Consider, by following the analysis in Wagner and Vella (2013), an inextensible and unshearable planar elastic rod with length L, resting on a rigid substrate (Fig. 1). We prescribe the distance between the ends of the rod and we consider the presence of a capillary adhesion, while we neglect gravity effects. We then solve the equilibrium equation and we compare the energies of the fully detached and partially attached solutions.

Let then $\mathbf{r}(s)$ be the position of a point of the curve representing the rod that can be parameterized by its Cartesian coordinates $\mathbf{r}(s) = x(s)\,\mathbf{e}_x + y(s)\,\mathbf{e}_y$, where s is the arc length. Denoting by $\theta(s)$ the angle between the tangent vector $\boldsymbol{\tau}(s)$ and the horizontal axis $\mathbf{e}_x$, the inextensibility constraint leads to $\boldsymbol{\tau}(s) = \mathbf{r}'(s) = \cos\theta(s)\,\mathbf{e}_x + \sin\theta(s)\,\mathbf{e}_y$, where a prime denotes differentiation with respect to s. Consequently,

$$x'(s) = \cos\theta(s), \qquad y'(s) = \sin\theta(s). \tag{1}$$

Under the simplifying assumption of symmetric solutions with respect to the y axis (see Fig. 1), we consider two possible non trivial equilibrium configurations: (i) the case where the rod is partially attached in two end point portions of length $L/2 - \bar{s}$ and detached in the middle portion of length $2\bar{s}$ (see Fig. 1(b)), and (ii) the case where the rod is fully detached as represented in Fig. 1(c).

We refer to the detached portion as *blister* and we determine its equilibrium shape as stationary points of the total energy functional (Wagner and Vella, 2013):

$$U(\theta(s), \theta'(s), \bar{s}) = \underbrace{2\int_0^{\bar{s}} \frac{k}{2}[\theta'(s)]^2 \mathrm{d}s}_{\text{bending}} \underbrace{- 2\int_{\bar{s}}^{\frac{L}{2}} \Delta\gamma\, \mathrm{d}s}_{\text{adhesion}} \underbrace{- 2\lambda\left[\int_0^{\frac{L}{2}} \cos\theta(s)\,\mathrm{d}s - a\right]}_{\text{end–end confinement}}, \tag{2}$$

where k is the bending stiffness, $\Delta\gamma$ the sheet–substrate adhesion energy density, and $2a$ is the constraint distance between the ends of the rod. The Lagrange multiplier λ, which ensures the geometrical condition of fixed distance between the end-points of the rods, measures the reaction force applied by the constraint at the end-points.

The equilibrium configuration descends by the Euler–Lagrange stationarity condition, and assigns the possible shapes of the blister:

$$k\,\theta''(s) - \lambda \sin\theta(s) = 0, \qquad s \in [0, \bar{s}]. \tag{3}$$

This equation may be recast as

$$\theta''(s) + \bar{\lambda}\sin\theta(s) = 0, \qquad s \in [0, \bar{s}], \tag{4}$$

where $\bar{\lambda} := -\lambda/k$. Note that both $\bar{\lambda}$ and $\bar{s}$ are unknowns.

2.1. Partially detached equilibrium solutions

Let us consider first the solutions represented in Fig. 1(b). In this case, we have to solve Eq. (4) supplied by the boundary conditions

$$\theta(0) = 0, \qquad \theta(\bar{s}) = 0 \tag{5}$$

and by the transversality condition (see *e.g.* Gelfand and Fomin, 1963), assigning the change of curvature at the detachment points,

$$\theta'(\bar{s}) = \frac{\sqrt{2}}{\ell_{\rm ec}}, \qquad \ell_{\rm ec} := \sqrt{\frac{k}{\Delta\gamma}}, \tag{6}$$

where $\ell_{\rm ec}$ represents the characteristic length of the system, here referred as *elastocapillary length* (Bico et al., 2004).

Eq. (4) admits the first integral

$$\frac{1}{2}[\theta'(s)]^2 - \bar{\lambda}\cos\theta(s) = C. \tag{7}$$

Denoting by s_0 the abscissa of the inflection point of the blister (*i.e.* $\theta'(s_0) = 0$) and by $\theta_0 := \theta(s_0)$, we obtain $C = -\bar{\lambda}\cos\theta_0$. On the other hand, by using Eq. (6), we obtain $C = \ell_{\rm ec}^{-2} - \bar{\lambda}$ and, hence, we deduce

$$\bar{\lambda} = \frac{1}{\ell_{\rm ec}^2}\frac{1}{1-\cos\theta_0}. \tag{8}$$

Consequently, Eq. (7) gives

$$[\theta'(s)]^2 = \frac{2}{\ell_{\rm ec}^2}\frac{\cos\theta(s) - \cos\theta_0}{1-\cos\theta_0}. \tag{9}$$

One can show (Wagner and Vella, 2013) that $s_0 = \bar{s}/2$ and that the portion of curve $s \in [s_0, \bar{s}]$ can be obtained by an in-plane rotation of π of the segment of the curve $s \in [0, \bar{s}_0]$. We also assume that $\theta(s)$ is a decreasing function for $s \in [0, s_0]$, so that (9) can be integrated by separation of variables

$$\int_0^{s_0} \mathrm{d}s = -\frac{\ell_{\rm ec}}{\sqrt{2}}\sqrt{1-\cos\theta_0}\int_0^{\theta_0}\frac{\mathrm{d}\theta}{\sqrt{\cos\theta - \cos\theta_0}}, \tag{10}$$

leading to

$$\bar{s} = -2\sqrt{2}\,\ell_{\rm ec}\,\mathrm{F}(q_0), \tag{11}$$

where F denotes the incomplete elliptic integral of first kind (Abramowitz and Stegun, 1964) and, for simplicity of notation, we set $q_0 = (\theta_0/2, \csc^2\theta_0/2)$.

Similarly, by denoting $\bar{x} := x(\bar{s})$, we have

$$\bar{x} = \int_0^{\bar{s}} \cos\theta(s)\,\mathrm{d}s = 2\int_0^{s_0} \cos\theta(s)\,\mathrm{d}s = -\ell_{\mathrm{ec}}\sqrt{2(1-\cos\theta_0)}\int_0^{\theta_0} \frac{\cos\theta\,\mathrm{d}\theta}{\sqrt{\cos\theta-\cos\theta_0}}, \tag{12}$$

whence we get

$$\bar{x} = -2\sqrt{2}\ell_{\mathrm{ec}}\left[(1-\cos\theta_0)E(q_0)+\cos\theta_0 F(q_0)\right], \tag{13}$$

where E denotes the incomplete elliptic integral of second kind.

Finally, by using the inextensibility constraint, we can obtain that $\bar{x} = a - (L/2 - \bar{s})$ that, combined with Eqs. (11) and (13), yields

$$a = \frac{L}{2} + 2\sqrt{2}\,\ell_{\mathrm{ec}}(1-\cos\theta_0)(\mathrm{F}(q_0)-\mathrm{E}(q_0)). \tag{14}$$

Eq. (14) can be solved numerically to obtain θ_0 as a function of the parameters L, a and ℓ_{ec}. Then, the obtained θ_0 can be replaced into Eq. (11) to obtain the length of the blister.

2.2. Fully delaminated configurations

Consider now the completely detached symmetric solution with only the ends of the rod, which are free to rotate, touching the substrate (see Fig. 1(c)). For these configurations, we have to solve Eq. (4) for $s \in [0, L/2]$, with the boundary conditions

$$\theta(0) = 0, \qquad \theta'(L/2) = 0, \tag{15}$$

where the second condition represents the condition of null moment at the ends.

By combining the boundary condition $(15)_2$ and the first integral (7), we get

$$[\theta'(s)]^2 = 2\,\bar{\lambda}\left(\cos\theta(s)-\cos\theta_f\right), \tag{16}$$

where $\theta_f := \theta(L/2)$. In the right-half portion of the rod, $s \in [0, L/2]$, we assume $\theta(s)$ to be a decreasing function, taking values between 0 and θ_f. Thus, Eq. (16) can be solved by separation of variables

$$\int_0^{\frac{L}{2}} \mathrm{d}s = -\frac{1}{\sqrt{2\bar{\lambda}}}\int_0^{\theta_f} \frac{\mathrm{d}\theta}{\sqrt{\cos\theta-\cos\theta_f}}, \tag{17}$$

yielding

$$L = -2\sqrt{\frac{2}{\bar{\lambda}}}\frac{\mathrm{F}(q_f)}{\sqrt{1-\cos\theta_f}}, \tag{18}$$

where $q_f := (\theta_f/2, \csc^2\theta_f/2)$. Since the distance between the ends of the rod is prescribed, we have

$$a = \int_0^{\frac{L}{2}} \cos\theta(s)\,\mathrm{d}s = -\frac{1}{\sqrt{2\bar{\lambda}}}\int_0^{\theta_f} \frac{\cos\theta\,\mathrm{d}\theta}{\sqrt{\cos\theta-\cos\theta_f}}, \tag{19}$$

whence we get

$$a = -\frac{\sqrt{2}}{\sqrt{\bar{\lambda}(1-\cos\theta_f)}}\left[(1-\cos\theta_f)E(q_f)+\cos\theta_f\mathrm{F}(q_f)\right]. \tag{20}$$

Eqs. (18) and (20) allow us to determine $\bar{\lambda}$ and θ_f as functions of the parameters L and a.

3. Results

We now compare the energies of the two considered equilibrium configurations. Let us begin by calculating the energy U_p of the partially delaminated configuration. By using Eq. (2) and the symmetry of the blister, we obtain

$$U_p = 4\int_0^{s_0} \frac{k}{2}[\theta'(s)]^2\mathrm{d}s - 2\Delta\gamma\left(\frac{L}{2}-\bar{s}\right). \tag{21}$$

By combining Eqs. (9) and (13), we get

$$\int_0^{s_0}[\theta'(s)]^2\mathrm{d}s = \int_0^{s_0}\frac{2}{\ell_{\mathrm{ec}}^2}\frac{\cos\theta-\cos\theta_0}{1-\cos\theta_0}\mathrm{d}s = \frac{1}{\ell_{\mathrm{ec}}^2}\frac{\bar{x}-\bar{s}\cos\theta_0}{1-\cos\theta_0}, \tag{22}$$

that replaced into (21) yields

$$U_p = \frac{2k}{\ell_{\mathrm{ec}}^2}\left(\frac{\bar{x}-\bar{s}\cos\theta_0}{1-\cos\theta_0}+\bar{s}-\frac{L}{2}\right) \tag{23}$$

and hence

$$U_p = \frac{2k}{\ell_{ec}^2}\left(\frac{a-L/2}{1-\cos\theta_0}+2\bar{s}-\frac{L}{2}\right). \tag{24}$$

The energy U_f of the fully delaminated solution is instead given by

$$U_f = k\int_0^{\frac{L}{2}}[\theta'(s)]^2\mathrm{d}s, \tag{25}$$

that, by using Eq. (16), reduces to

$$U_f = k\int_0^{\frac{L}{2}} 2\bar{\lambda}\left(\cos\theta(s)-\cos\theta_f\right)\mathrm{d}s \tag{26}$$

and finally

$$U_f = k\,\bar{\lambda}\,(2a - L\cos\theta_f). \tag{27}$$

We now compare the energies (24) and (27). To this end, we first introduce the dimensionless confinement and elastocapillary parameters

$$\varepsilon := \frac{L-2a}{L}, \qquad \xi_{\mathrm{ec}} := \frac{\ell_{\mathrm{ec}}}{L} \tag{28}$$

and the dimensionless energies

$$u_p := \frac{U_p L}{k} = -\frac{1}{\xi_{\mathrm{ec}}^2}\left[\frac{\varepsilon}{1-\cos\theta_0}+\left(1-\frac{4\bar{s}}{L}\right)\right], \tag{29a}$$

$$u_f := \frac{U_f L}{k} = hL^2(1-\varepsilon-\cos\theta_f). \tag{29b}$$

In Fig. 2 (left), we represent the energies u_p (blue curves) and u_f (red curve) as functions of the dimensionless confinement ε, for different values of ξ_{ec}. As ε increases from zero, a critical threshold is reached above which the fully delaminated solution corresponds to the absolute minimum of the energy. This threshold grows as the energy of adhesion increases (ξ_{ec} decreasing).

The set of critical thresholds obtained by varying ξ_{ec} defines the curve in the plane of parameters $(\xi_{\mathrm{ec}}, \varepsilon)$ corresponding to the phase diagram represented in Fig. 2 (right). As expected, the critical strain at the which the rods completely delaminates is an increasing function of the adhesion energy.

To better understand the behavior of the critical curve, we consider the asymptotic expansion for $\varepsilon \ll 1$ of the above obtained equations. These developments, which we do not detail here, use the approximations for elliptic integrals given in Wagner and Vella (2013) . Thus, at the leading order, we obtain a simple (but effective) formula

$$\varepsilon_{\mathrm{cr}} \approx \frac{1}{27\pi^2\xi_{\mathrm{ec}}^2}, \tag{30}$$

which is represented by the dashed curve in Fig. 2 (right). Interestingly, Eq. (30) provides a very good account of the numerical results for the whole range before the first self-contact point. This equation can then be considered as a simple relation assigning the critical condition indicated in the introduction for possible applications in actuation and sensing devices, or, in the spirit of Wagner and Vella (2013), as a relation to accurately measure the capillarity energy density $\Delta\gamma$.

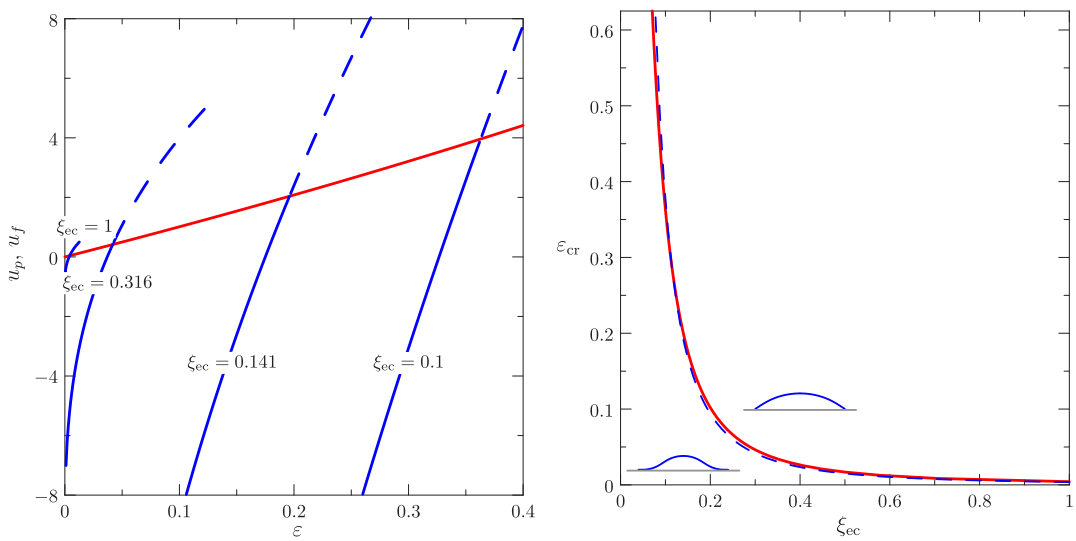

Fig. 2. (Left) Energy function for the partially detached solutions u_p (blue curves), at variable ξ_{ec}, and for the fully detached solution u_f (red curve), as functions of the constraint measure ε. The lower limit for any blue curves is $-\xi_{ec}^{-2}$, whereas the upper limit corresponds to the first self-contact point. (Right) Critical confinement ε_{cr} as a function of the elastocapillary parameter ξ_{ec}. The solid curve represents numerical result, while the dashed curve represents the asymptotic result provided by Eq. (30). (For interpretation of the references to color in this figure legend, the reader is referred to the web version of this article.)

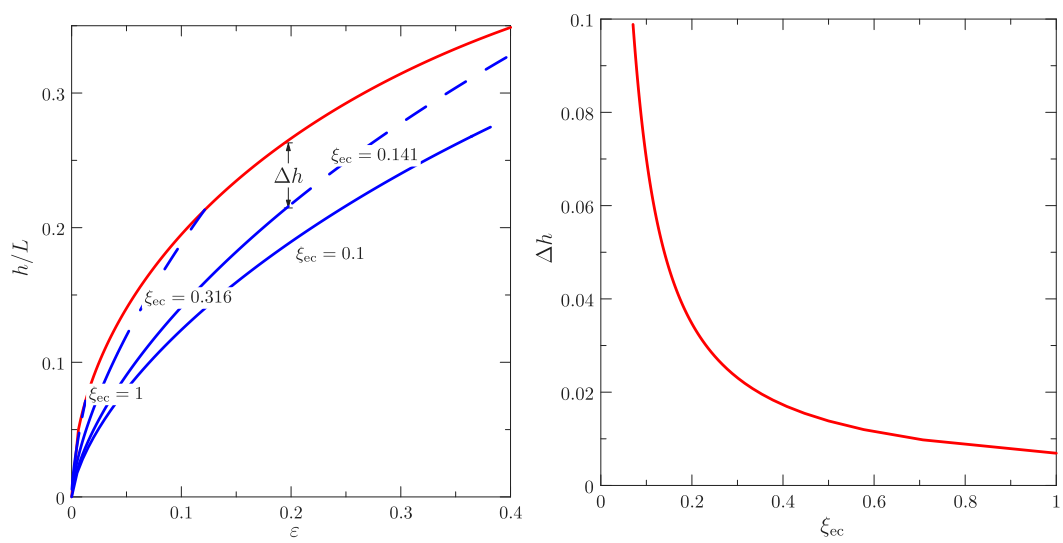

Fig. 3. (Left) Maximum displacement h as a function of the confinement measure ε. Blue curves represent h_p/L at different values of ξ_{ec}, while the red curve represent h_f/L. Δh measures the difference between the maximum displacements at the critical threshold. (Right) Δh as a function of the elastocapillary parameter ξ_{ec}. (For interpretation of the references to color in this figure legend, the reader is referred to the web version of this article.)

More in detail, we may observe that as ε grows, the transition occurs discontinuously, with the solution abruptly switching from the partially delaminated to the fully detached state. In order to give a measure of such effect, we can integrate Eq. $(1)_2$ to obtain the height h of the symmetry point ($s = 0$). Thus, for the partially detached solution, we have

$$h_p = -2\int_0^{s_0} \sin\theta(s)\,\mathrm{d}s, \tag{31}$$

that, with the use of Eq. (9), reduces to

$$h_p = \ell_{ec}\sqrt{2(1-\cos\theta_0)}\int_0^{\theta_0} \frac{\sin\theta\,\mathrm{d}\theta}{\sqrt{\cos\theta-\cos\theta_0}} \tag{32}$$

and, therefore,

$$h_p = 2\sqrt{2}\,\ell_{ec}\left(1-\cos\theta_0\right). \tag{33}$$

In a similar way, we can use Eqs. $(1)_2$ and (16) to obtain the height of the middle point of the completely detached solution:

$$h_f = -\int_0^{\frac{L}{2}} \sin\theta(s)\,\mathrm{d}s = \frac{1}{\sqrt{2\bar{\lambda}}}\int_0^{\theta_f} \frac{\sin\theta\,\mathrm{d}\theta}{\sqrt{\cos\theta-\cos\theta_f}} = \sqrt{\frac{2(1-\cos\theta_f)}{\bar{\lambda}}} \tag{34}$$

Fig. 3 (left) sketches h_f/L (red curve) and h_p/L (blue curves) for several values of ξ_{ec}. Both these quantities increase as the ends approach each other. At the critical threshold (end of continuous curve) the difference $\Delta h := (h_f - h_p)/L$, is finite. Fig. 3 (right) shows Δh as a function of the parameter ξ_{cr}.

Finally, we observe that also the internal force $\bar{\lambda}$ undergoes a finite jump at the critical threshold. In particular, from switching from the partially adhered to the fully detached solution, $\bar{\lambda}$ suddenly decreases as Fig. 4 (left) shows. This jump increases with the adhesion energy (Fig. 4 (right)).

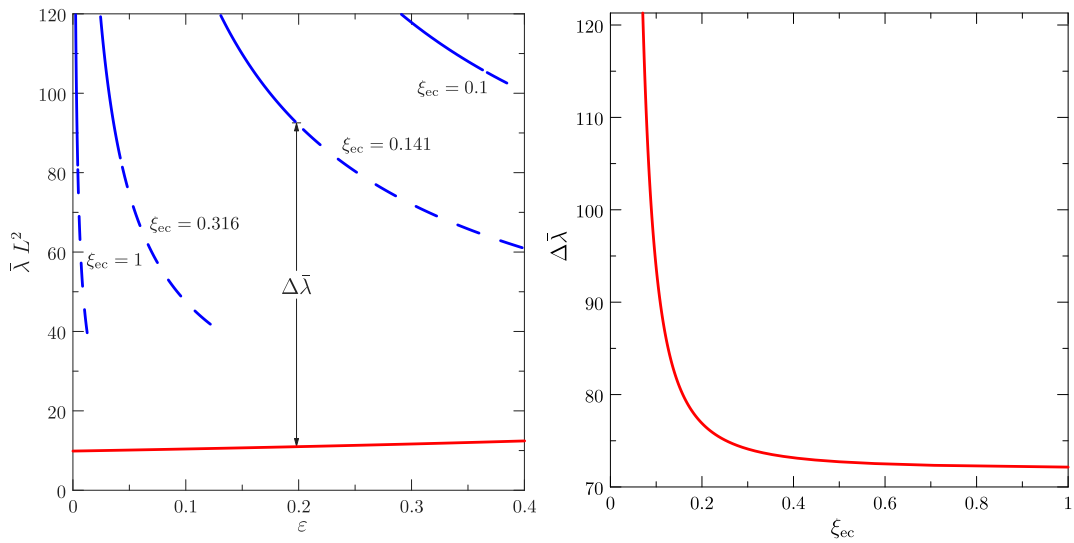

Fig. 4. (Left) Dimensionless Internal force $\bar{\lambda}L^2$ as a function of the confinement measure ε. Blue curves represent partially adhered configurations at different values of ξ_{ec}, while the red curve represent the completely detached solution. $\Delta\lambda$ measures the jump of force at the critical threshold. (Right) $\Delta\bar{\lambda}$ as a function of the elastocapillary parameter ξ_{ec}. (For interpretation of the references to color in this figure legend, the reader is referred to the web version of this article.)

4. Conclusions

Technologies at small scales such as MEMS and NEMS, as well as biological systems in soft materials, suggest many applications relying on the possibility of actively controlling adhesion devices based on delamination phenomena. In typical devices the delaminated components undergo large deflection with the involvement of nonlinear effects. Our approach combines a simple model of adhesion and the Euler's elastica to study the transition between partially adhered to completely delaminated states of an elastic rod with end–end confinements. In order to well describe these effects, the interaction between the involved elastic and adhesion energy and the resulting equilibrium conformations must be analyzed.

Our study, which uses closed-form solutions of the equilibrium equations, is complementary to other studies in the literature investigating the early stages of delamination (Wagner and Vella, 2013; Napoli and Turzi, 2017; Davidovitch and Démery, 2021). We show that there exists an initial stage when as the compression is increased the system is partially detacched with the size of the blister of the partially delaminated solution increasing continuously until the confinement reaches a critical value. Beyond this critical threshold, the partially adhered solution becomes unstable (or metastable), while the fully delaminated configuration represents the absolute minimum of the energy. Using asymptotic calculation, we also provide a simple formula for the critical threshold that is in excellent agreement with the numerical results that can deliver a simple design approximation. Furthermore, our result highlight a sudden change of shape, with a discontinuous transition in terms of equilibrium configurations and of the involved forces.

In the light of our findings, we may speculate that our system can be a prototypical device of controlled adhesion. Indeed it is possible to actively control the parameter ξ_{ec} by electromechanical adhesion systems or the parameter ε by a thermal or chemical external field. The existence of the obtained relevant morphological and force discontinuities in correspondence of the critical thresholds enables different applications in the fields of sensoring and actuation. We may also suppose that such kind of instability thresholds can be used for accurate measurement of capillary adhesion (Wagner and Vella, 2013). Finally we may argue that important growth-induced decohesion instabilities in the biological field can also be described within the proposed framework.

Declaration of competing interest

The authors declare that they have no known competing financial interests or personal relationships that could have appeared to influence the work reported in this paper.

Acknowledgments

The authors acknowledge the financial support by the MIUR (Italian Ministry of Education, University and Research) project PRIN 2017, *Mathematics of active materials: From mechanobiology to smart devices*, project no. 2017KL4EF3 and GNFM of Italian INdAM.

References

Abramowitz, M., Stegun, I.A., 1964. Handbook of Mathematical Function with Formulas, Graphs, and Mathematical Tables. Dover, New York.
Arazoe, H., et al., 2016. An autonomous actuator driven by fluctuations in ambient humidity. Nature Mater. 15, 1084–1089.
Bico, H., Roman, B., Boudaoud, A., 2004. Elastocapillary coalescence in wet hair. Nature 432 (7018), 690.
Cerda, E., Mahadevan, L., 2005. Confined developable elastic surfaces: cylinders, cones and the elastica. Proc. R. Soc. Lond. Ser. A Math. Phys. Eng. Sci. 461 (2055), 671–700.
Coclite, G.M., Florio, G., Ligabò, M., Maddalena, F., 2019. Adhesion and debonding in a model of elastic strings. Comput. Math. Appl. 78, 1897–1909.
Davidovitch, B., Démery, V., 2021. Rucks and folds: delamination from a flat rigid substrate under uniaxial compression. Eur. Phys. J. E 44 (2), 11.
De Pascalis, R., Napoli, G., Turzi, S.S., 2014. Growth-induced blisters in a circular tube. Physica D 283, 1–9.
De Tommasi, D., Devillanova, G., Maddalena, F., Napoli, G., Puglisi, G., 2021. Elastic multi-blisters induced by geometric constraints. Proc. R. Soc. A: Math. Phys. Eng. Sci. 477 (2245), 20200562.
Domokos, G., Fraser, W.B., Szeberényi, I., 2003. Symmetry-breaking bifurcations of the uplifted elastic strip. Physica D 185 (2), 67–77.
Douglas, Graeham R., Srikantha Phani, A., Gagnon, Jöel, 2014. Analyses and design of expansion mechanisms of balloon expandable vascular stents. J. Biomech. 47 (6), 1438–1446.
Gelfand, I.M., Fomin, S.V., 1963. Calculus of Variations. Prentice Hall.
Goriely, A., 2017. The Mathematics and Mechanics of Biological Growth. Springer Verlag, New York.
Ke, C., Zheng, M., Bae, I., Zhou, G., 2010. Adhesion-driven buckling of single-walled carbon nanotube bundles. J. Appl. Phys. 107, 104305.
Kim, D.-H., Xiao, J., Song, J., Huang, Y., Rogers, J.A., 2020. Stretchable, curvilinear electronics based on inorganic materials. Adv. Mater. 22 (19), 2108–2124.
Lu, N., Kim, D.-H., 2020. Flexible and stretchable electronics paving the way for soft robotics. Soft Robot. 1 (1), 53–62, 07/03 2013.

Maddalena, F., Percivale, D., Puglisi, G., Truskinowsky, L., 2009. Mechanics of reversible unzipping. Contin. Mech. Thermodyn. 21, 251–268.
Maddalena, F., Percivale, D., Tomarelli, F., 2012. Adhesive flexible material structures. Discrete Contin. Dyn. Syst. Ser. B 17 (553–574).
Majidi, C., 2007. Remarks on formulating an adhesion problem using euler's elastica (draft). Mech. Res. Commun. 34 (1), 85–90.
Napoli, G., Goriely, A., 2017. A tale of two nested elastic rings. Proc. R. Soc. Lond. Ser. A Math. Phys. Eng. Sci. 473 (2204).
Napoli, G., Turzi, S., 2015. Snap buckling of a confined thin elastic sheet. Proc. R. Soc. Lond. Ser. A Math. Phys. Eng. Sci. 471 (2183), 20150444.
Napoli, G., Turzi, S., 2017. The delamination of a growing elastic sheet with adhesion. Meccanica 52 (14), 3481–3487.
Oshri, O., 2020. Delamination of open cylindrical shells from soft and adhesive winkler's foundation. Phys. Rev. E 102, 033001.
Oshri, O., Liu, Y., Aizenberg, J., Balazs, A.C., 2018. Delamination of a thin sheet from a soft adhesive winkler substrate. Phys. Rev. E 97 (6), 062803–062806.
Petrik, V., Smutny, V., Kyrki, V., 2020. Static stability of robotic fabric strip folding. IEEE/ASME Trans. Mechatronics 1.
Pocivavsek, L., Pugar, J., O'Dea, R., Ye, S.-H., Wagner, W., Tzeng, E., Velankar, S., Cerda, E., 2018. Topography-driven surface renewal. Nat. Phys. 14 (9), 948–953.
Puglisi, G., Truskinovsky, L., 2013. Cohesion-decohesion asymmetry in geckos. Phys. Rev. E 87 (3), 032714.
Que, L., Park, J.-S., Gianchandani, Y.B., 1999. Bent-beam electro-thermal actuators for high force applications. In: Technical Digest. IEEE International MEMS 99 Conference. Twelfth IEEE International Conference on Micro Electro Mechanical Systems (Cat. No. 99CH36291). IEEE.
Shintake, J., et al., 2016. Versatile soft grippers with intrinsic electroadhesion based on multifunctional polymer actuators. Adv. Mater. 28, 231–238.
Sun, Y., Choi, W.M., Jiang, H., Huang, Y.Y., Rogers, J.A., 2006. Controlled buckling of semiconductor nanoribbons for stretchable electronics. Nat. Nanotech. 1 (3), 201–207.
Turzi, S., Zoppello, M., Ambrosi, D., 2021. Equilibrium of two rods in contact under pressure. Quart. J. Mech. Appl. Math. 73 (4), 329–346.
Vella, D., Bico, J., Boudaoud, A., Roman, B., Reis, P.M., 2009. The macroscopic delamination of thin films from elastic substrates. Proc. Natl. Acad. Sci. USA 106 (27), 10901–10906.
Wagner, T.J.W., Vella, D., 2013. The 'sticky elastica': delamination blisters beyond small deformations. Soft Matter 9 (4), 1025–1030.
Wang, H., Yamamoto, A., 2017. Analyses and solutions for the buckling of thin and flexible electrostatic inchworm climbing robots. IEEE Trans. Robot. 33 (4), 889–900.
Wu, J., et al., 2011a. Mechanics of reversible adhesion. Soft Matter 18, 8657–8662.
Wu, J., et al., 2011b. Mechanics of reversible adhesion. Soft Matter 7, 8657.
Wyatt, T.P.J., et al., 2020. Actomyosin controls planarity and folding of epithelia in response to compression. Nature Mater. 29, 109–117.